Chem

CellPress

Article

Logic operation and real-time communication via tunable excited states in a single-molecule optoelectronic chip

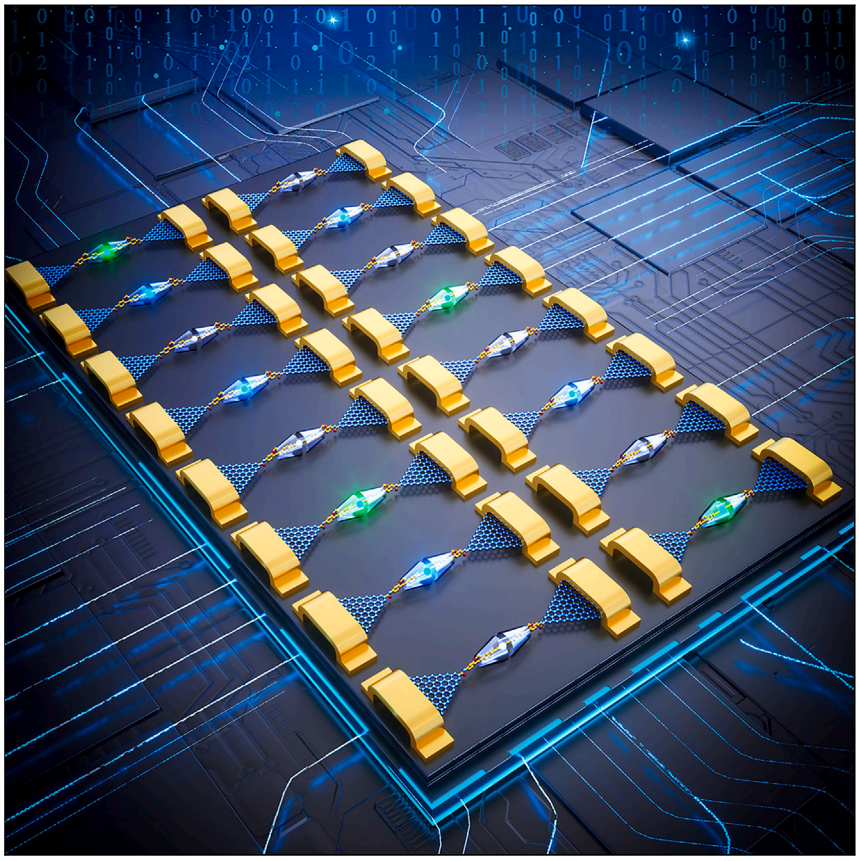

A highly integrated single-molecule optoelectronic device on chip enables binary and trinary logic operations as well as real-time communication and display.

Chen Yang, Yilin Guo, Hiroshi Masai, ..., Hongmei Su, Jun Terao, Xuefeng Guo

cterao@g.ecc.u-tokyo.ac.jp (J.T.)
guoxf@pku.edu.cn (X.G.)

Highlights

Compatibility between excitation lifetime and efficiency in an individual molecule

Selective phosphorescence or fluorescence emission in an individual molecule

Logic operation and real-time communication achieved by a single-molecule device

Yang et al., Chem *10*, 1445–1457
May 9, 2024
https://doi.org/10.1016/j.chempr.2024.01.005

Chem

CellPress

Article

Logic operation and real-time communication via tunable excited states in a single-molecule optoelectronic chip

Chen Yang,[1,5] Yilin Guo,[1,5] Hiroshi Masai,[2] Tomohiro Iwai,[2] Jialong Jie,[3] Hongmei Su,[3] Jun Terao,[2,*] and Xuefeng Guo[1,4,6,*]

SUMMARY

The preparation of single-molecule optoelectronic devices has been considered as one of the most promising strategies to adhere to Moore's law. Yet, to date, individual molecules have not rivaled semiconductors in terms of device performance and stability. Here, we introduce two cyclodextrins to encapsulate a molecular bridge, a new strategy in molecular and device engineering, to create a robust graphene-based single-molecule optoelectronic chip. By isolating single molecules from the environment, a high quantum yield (10^{-6}) and ultra-long phosphorescence lifetime (millisecond scale) can be achieved at a platinum-centered single-molecule junction. On the basis of a single-molecule transient electroluminescence spectroscopy, tunable singlet and triplet excited states are directly observed by multimode electrical inputs. Further regulation of fluorescence and phosphorescence and selective emission enable comprehensive binary and trinary logical operations, as well as real-time communications. The presented multifunctional, efficient single-molecule optoelectronic device can help link conceptual molecular electronics to practical semiconductors.

INTRODUCTION

The use of a single molecule to build an electronic device is a strategy to adhere to Moore's law and satisfy the increasing demands of device miniaturization.[1] As the building block of the nanoscale circuit, various functional units can be engineered by organic synthesis, i.e., molecular engineering.[2,3] In this regard, theoretically proposed molecules have been synthesized and integrated into nanogapped electrodes to enable corresponding functions.[4–9] On the other hand, of equal importance is device engineering, involving electrode and molecule-electrode interface, which enables the high performance of molecules.[3,10,11]

However, to date, one individual molecule has not rivaled semiconductors in terms of device performance and stability,[12] including the on/off ratio of field-effect transistors,[13–15] the quantum yield of light-emitting diodes,[16–18] and the operating frequency of a corresponding logic circuit.[19–21] The interactions between the molecule and environment (including the electrode, chip substrate, and surrounding gas or solvent molecules; i.e., the interface coupling) are a leading cause of this insufficient performance.[3] Specifically, strong coupling leads to the superposition of molecular binary states (e.g., on/off states or excited/ground states) with the wavefunction of the environment and to a series of perturbed molecular states. This reduces the corresponding on/off ratio or increases nonradiative deactivation. In contrast, weak coupling weakens the modulation by external

THE BIGGER PICTURE

Using single-molecule devices as basic electronic components is a non-trivial task. Here, we report not just the implementation of practical single-molecule devices but also an unprecedentedly precise manipulation of single-molecule behaviors, including excited-state dynamics, excitation lifetime, and efficiency. These advances offer a strategy to design high-performance optoelectronic materials and a crucial step toward the real, practicable development of optoelectronic devices that use single-molecule optoelectronic properties. In combination with the high stability of this covalent-bond electrode-molecule interface and the on-chip setup, we believe that this single-molecule device is one of the most potential candidates for practical applications.

stimuli as well as the corresponding operating frequency. A compromise in these aspects necessitates further development in molecular and device engineering. The choice of molecule and electrode, atomic-scale configuration of the electrode, molecule-electrode interface, robustness of the device, and molecular isolation from the external environment should be considered holistically.

Herein, we report a multifunctional single-molecule optoelectronic device consisting of a cyclodextrin (CD)-encapsulated, platinum (Pt)-centered molecular bridge (Pt-MB@CD) (or a control molecular bridge without CD [Pt-MB]; the detailed molecular structure is provided in Scheme S1), nanogapped graphene electrodes, and covalent amide linkages on a Si wafer substrate. These transition metal complexes with π-conjugated ligands are well known because of their fluorescence and phosphorescence. In detail, the π-conjugated ligands enable effective radiation originating from the metal-to-ligand charge transfer and π–π* transitions. The heavy atom Pt provides an effective transition from the singlet state to the triplet state and the direct relaxation to the ground state from the triplet state due to the large spin-orbital coupling, which provides multiple states for logic operation and information transmission. The two CDs on both sides weaken the coupling with the environment and thus avoid corresponding non-radiative processes. Graphene electrodes enable a robust covalent interface with molecules and further multimolecular integration. This on-chip setup is compatible with commercial complementary metal-oxide-semiconductor technology and various electrical inputs, which is important to impart various functions (Figure 1A).

Results and discussion

Characterization of a single-molecule optoelectronic chip

To prepare the device, the graphene ribbon between the metal electrodes (source and drain) was etched with oxygen plasma in accordance with a dash-line pattern to prepare nanoscale gaps with carboxyl terminals at both sides (exhibiting an open circuit; Figure 1B).[22] The molecular bridge with amine end groups was integrated into the electrodes via amide bonds. Detailed synthetic procedures and structural characterizations of the molecular bridges are provided in the supplemental information. Further optical characterization indicates both fluorescent and phosphorescent emissions (Figures S1–S5), laying the foundation for preparing single-molecule optoelectronic chips. Recovery of the conductance between the source and drain electrodes indicates the molecular connection (showing the single-molecule junction [SMJ], Figure 1B). The supplemental information provides detailed information on preparing the single-molecule device. Under the optimized conditions, ∼30 of 169 devices exhibited a current response versus bias voltage (Figure S6), indicating that the connection yield reached ∼18%. The statistical analysis results reported in the supplemental information indicate that the current response, ∼91% probability, originated from the only-one-molecule connection between the electrodes. Furthermore, electroluminescence (voltage between the source and drain (V_{SD}) = 3.5 V) could be characterized by super-high-resolution imaging. The molecular site can be localized via the stochastic optical reconstruction microscopy (STORM),[23] again demonstrating the single-molecule connection (Figure 1C).

The present molecular bridge with a heavy atom center (Pt) enables spin-forbidden phosphorescence emission and thus high electroluminescence efficiency beyond the spin statistics limitation (25%) by taking advantage of the remaining 75% triplet excitons. Multistate switching was observed during current-voltage ($I-V$) scanning (Figure 1B), implying a multimodal photophysical process. Understanding the detailed mechanism requires further characterization, especially synchronous optical and electrical measurements. The chip was encapsulated by deoxygenated

[1]Beijing National Laboratory for Molecular Sciences, National Biomedical Imaging Center, College of Chemistry and Molecular Engineering, Peking University, 292 Chengfu Road, Haidian District, Beijing 100871, P.R. China

[2]Department of Basic Science, Graduate School of Arts and Sciences, The University of Tokyo, Tokyo 153-8902, Japan

[3]Collage of Chemistry, Beijing Normal University, 19, Xinjiekouwai Street, Haidian District, Beijing 100875, P.R. China

[4]Center of Single-Molecule Sciences, Institute of Modern Optics, Frontiers Science Centre for New Organic Matter, College of Electronic Information and Optical Engineering, Nankai University, 38 Tongyan Road, Jinnan District 300350, Tianjin, P.R. China

[5]These authors contributed equally

[6]Lead contact

*Correspondence: cterao@g.ecc.u-tokyo.ac.jp (J.T.), guoxf@pku.edu.cn (X.G.)

https://doi.org/10.1016/j.chempr.2024.01.005

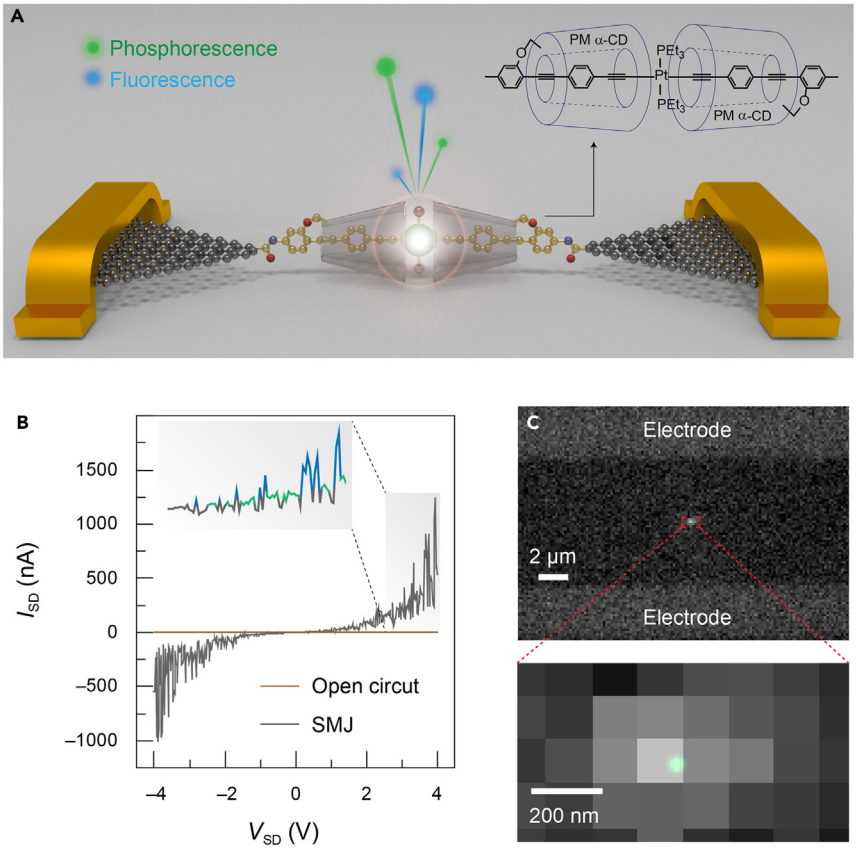

Figure 1. Characterization of a single-molecule Pt-MB@CD device

(A) Schematic of a single-molecule device, including the molecular structure, indicating the phosphorescence and fluorescence emissions.

(B) *I*–*V* scans ranging from −4 to 4 V before (open circuit) and after single-molecule connection (SMJ). Inset shows the enlarged images from 2.5 to 4 V. The SMJ was encapsulated with deoxygenated polydimethylsiloxane before measurement to prevent electrical burning at a high bias voltage and the oxygen quenching of the phosphorescence. Peak fluctuation of the *I*–*V* curves of the SMJ implies switching among three inherent molecular states (*vide infra*).

(C) Super-high-resolution optical imaging of the single-molecule device and a corresponding enlarged image under V_{SD} = 3.5 V; V_{SD}, bias voltage between the source and drain.

polydimethylsiloxane (PDMS) to prevent electrical burning at a high bias voltage and the oxygen quenching of the phosphorescence (the covalent anchoring stabilizes the luminous center before and after encapsulation); the current-time (*I*–*t*) curve at V_{SD} = 3.0 V and the corresponding recorded photons are provided in Figure 2A. Three discrete current states and two special photons with different wavelengths (i.e., fluorescence, ~410 nm and phosphorescence, ~524 nm) were mainly obtained (Figures 2B and 2C). The emitted photons are in line with macroscopic measurements of this molecule,[24,25] indicating a relatively "pure molecular state" between the electrodes, which originates from the isolation by using CDs and the atomic-scale triangular geometry of the etched graphene electrode. In addition, the single-molecule setup prevents triplet-triplet annihilation, and the phosphorescent material could be adopted individually with high-density integration on a chip to prepare highly efficient light-emitting diodes.[26]

A strong statistical correlation between the emitted photons and current changes (I_N – I_{N+1}) was observed (Figure 2D), which can be assigned to the corresponding states,

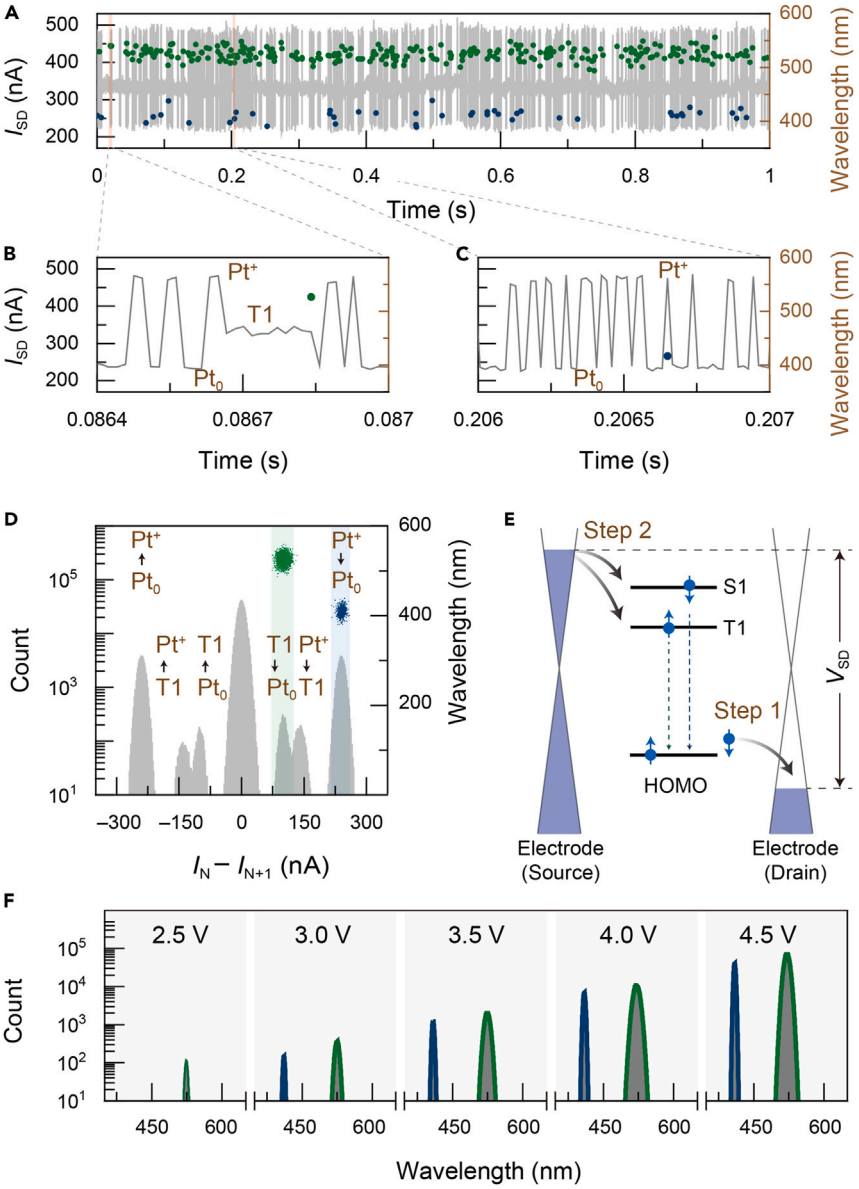

Figure 2. Optic-electrical synchronous characterizations of a single-molecule Pt-MB@CD device and corresponding electroluminescence mechanism

(A) Synchronous measurements of the optical and electrical signals at V_{SD} = 3.0 V. V_{SD}, bias voltage between the source and drain.

(B and C) Enlarged images to indicate the correlation between the emitted photons and conductance states.

(D) Statistics of the conductance-switching sequence and photon emission. Specifically, the histogram distribution analysis of the current is based on the values of the previous data point (I_N) minus the next point (I_{N+1}). Then, the direct conversions from one conductance to another were extracted as several peaks. Therein, the conversion from ~480 (I_N) to ~250 (I_{N+1}) nA corresponds to the emission of fluorescence ($I_N - I_{N+1}$ = ~ +230 nA), whereas the conversion from ~340 (I_N) to ~250 (I_{N+1}) nA corresponds to the emission of phosphorescence ($I_N - I_{N+1}$ = ~ +90 nA).

(E) Electron transmission mechanism as well as the corresponding phosphorescence and fluorescence emissions.

(F) Statistics of the photon numbers and energy with various bias voltages.

including the triplet (marked as T1) and ground (marked as Pt_0) states. The singlet states cannot be directly observed by an electrical signal due to its short lifetime.[24] The corresponding current changes that enable the emission of fluorescence photons can be assigned to the transformation from the positive-charged state (Pt^+) to Pt_0. In detail, Figure 2E describes the corresponding scenarios upon the application of bias voltage. An electron jumping from the highest occupied molecular orbital (HOMO) to the drain electrode leads to a measurable positive-charged state. The gate-voltage-dependent measurement further supports the assignment of this Pt^+ state[14,27] (Figure S7). The subsequent electron injected from the source electrode could fill the HOMO, singlet state, or triplet state, among which the short-lived singlet state relaxes to the initial Pt_0 state, concomitant with rapid photon emission. The further V_{SD}-dependent measurement demonstrates the energy difference between the singlet and triplet states (directly formed by electron injection, Figure 2F). The lower triplet state can be formed selectively at $V_{SD} < 3$ V, whereas both the singlet and triplet states can be formed at a higher V_{SD}. These tunable multimodal photophysical processes afford multistate logic operation and information transformation (*vide infra*). The statistics of the photon number within 1 s indicate a quantum yield of up to $\sim 10^{-6}$ at $V_{SD} = 4.5$ V (Figure 2F), which is three orders of magnitude higher than those in other carbon-based single-molecule devices without plasma enhancement,[28] the device without molecule-scale encapsulation ($\sim 10^{-10}$ to 10^{-9}),[17,18,29] and the Pt-MB device ($\sim 10^{-9}$, Figure S8). The high quantum yield is attributable to the isolation of the luminous center from the external environment with two CDs. Unlike the macroscopic scale at which intermolecular interactions induce quenching, the insulation of Pt-MB by CDs effectively blocked the electron and energy transfer between the excited state and substrate/surrounding molecules, therefore enabling a more effective radiative transition. In addition, with the application of a high bias voltage (4.5 V), both kinds of devices showed high stability due to the covalent interface. No obvious fluctuations of the emitted photon numbers and corresponding efficiency were observed during 120 h (Figures S9 and S10).

The "mixed state" of the molecule was also observed in the junction. The narrower fluorescence and phosphorescence emission spectra than those at the macroscopic level[25] originate from the covalent anchor of the molecular bridge, as well as the limitation of corresponding vibration modes. Similarly, the restriction of the conformation imparted by using CDs[30] and electrodes resulted in a slower vibrational relaxation rate than the photon emission, which led to the blue shift of the emission peak.[25] This is similar to some cases where macroscopic molecules are located in a rigid or high-viscosity solution.[31] The phosphorescence lifetime was further characterized by a single-molecule transient electroluminescence spectroscopy (sm-TES). A 555-picosecond-wide pulse with a 2.5-V amplitude was applied between the source and drain (Figure 3A), and the emitted phosphorescence photons were detected synchronously with a single-photon counter. The typical current and emitted photons were plotted in Figure 3B and enlarged in Figure 3C. The sm-TES excludes the exciton diffusion in bulk materials and provides inherent excited-state characteristics.[32] The time intervals between the captured photons and applied electrical pulse were extracted, and the corresponding statistical distribution is provided in Figure 3D. Because of the zero-field splitting of the triplet state (Figure 3E), in comparison with the single-exponential fitting, the triple-exponential fitting agrees better with the datum points and indicates the characteristic lifetimes of ~1.35, ~4.45, and ~10.50 ms. These phosphorescent lifetimes are much higher than those at the macroscopic scale (Figures S4 and S5) and in other derivatives.[24] Therefore, we could summarize that the longer lifetimes of both Pt-MB (Figure 3F) and Pt-MB@CD result from the limitation of the molecular motion, vibration, and rotation modes (that suppress the dissipation of the excited-state energy). In addition, the only-one-molecule setup essentially avoids triplet-triplet annihilation. In addition, the phosphorescence lifetimes can be directly obtained from the real-time-monitored current during electrical input (Figures 2A and 2B). A

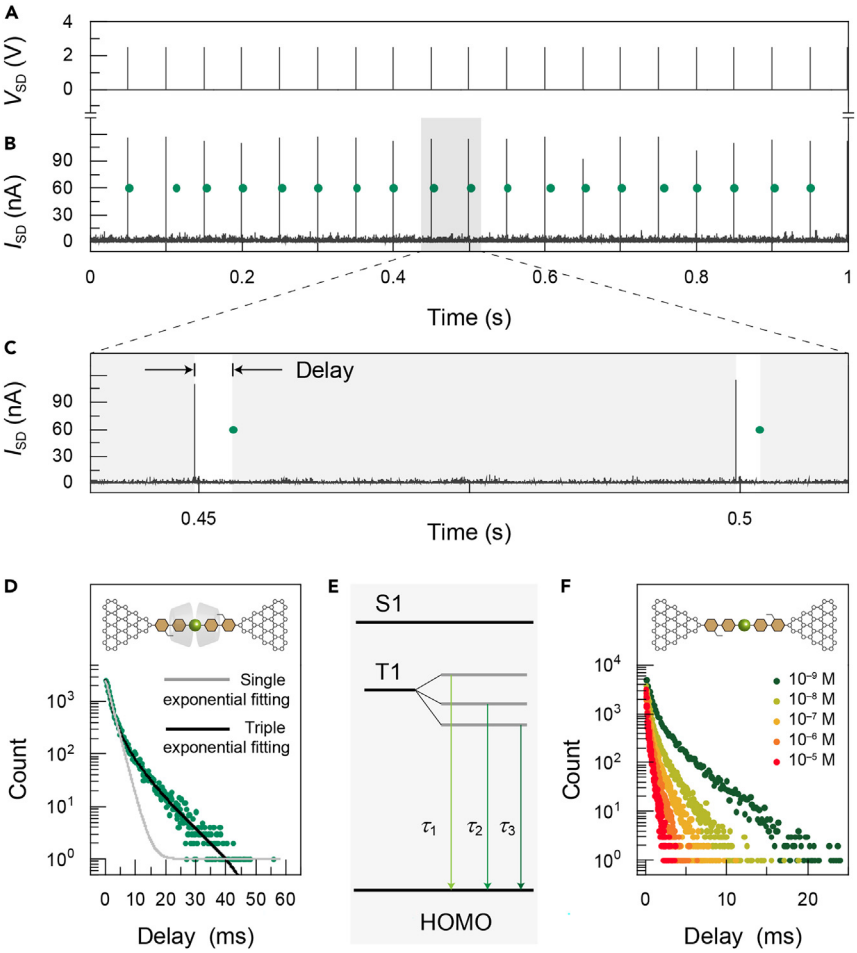

Figure 3. Single-molecule transient electroluminescence spectroscopy for measuring the phosphorescence lifetime

(A) Input sequence of the bias voltage.

(B) Typical synchronously recorded current signal and emitted phosphorescent photon signal of the single-molecule Pt-MB@CD device. Some electrical pulses are followed by photons, which are collected by the single-photon avalanche diode after filtering light below 458 nm (to ensure the phosphorescent photon collection). Therefore, one green dot here indicates one collected phosphorescent photon.

(C) Enlarged image of (B) that indicates the decay between the phosphorescence emission and electrical pulse input.

(D) Statistical histogram of the decay time extracted from (B) and corresponding fitting with single- and triple-exponential curves, respectively.

(E) Schematic of the zero-field splitting of the triplet state.

(F) External heavy atoms mixed the molecular state without isolation by using CDs (single-molecule Pt-MB device) and the corresponding regulation of the phosphorescence lifetime. Iodoethane (10^{-9} M ~ 10^{-5} M) was added from the outside via mixing with uncured PDMS.

reduction of the phosphorescence lifetimes was observed accompanied by an increased bias voltage (Figures S11 and S12). Considering the opening of additional vibrational modes of the molecule when the current flows through a single molecule, i.e., electron-phonon coupling,[33] the shorter lifetime of the phosphorescence at high bias could be attributed to the increased overlap between T1 and Pt_0 states and spin-orbital coupling.[34] The regulation of the phosphorescence lifetimes facilitates new opportunities for compatibility between quantum yield and ultra-long phosphorescence in one device. In addition to the bias voltage, the phosphorescence lifetimes can be regulated with an external

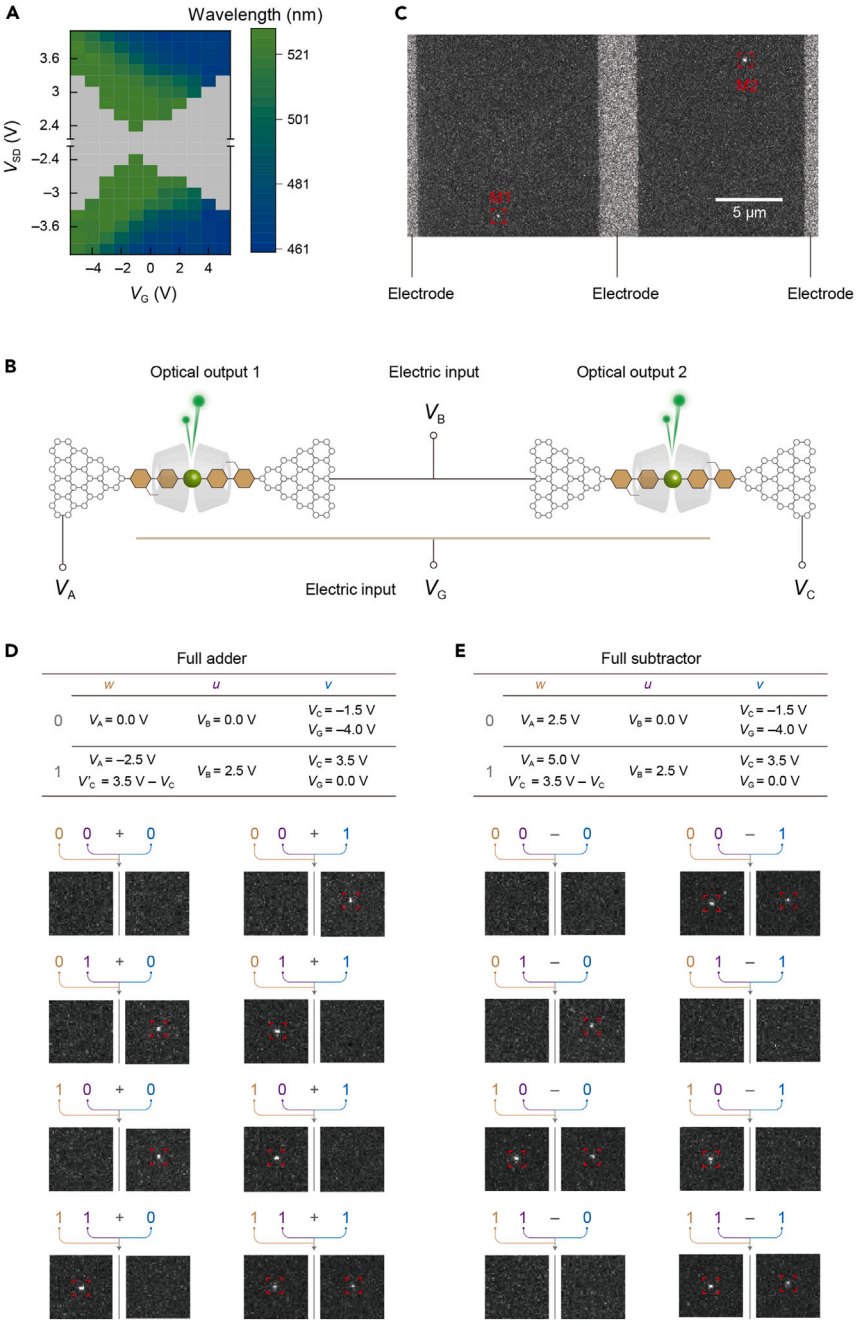

Figure 4. Binary logic operations with a single-molecule Pt-MB@CD device

(A) Two-dimensional mapping of emitted photons with V_G-V_{SD}-dependent inputs. $V_{SD} = V_S - V_D$. Statistical (averaged) wavelengths of phosphorescence and fluorescence (over 10 s) were obtained by location on the Commission International de l'Eclairage (CIE) chromaticity standard.

(B) Schematic of two single-molecule devices to enable the combination of basic logic gates.

(C) Optical image of two single-molecule devices with V_B and V_G = 0 V and V_A and V_C = 2.5 V.

(D) Construction of the full-adder, in which *u* and *v* serve as the two addends and *w* is the carry-in. Corresponding threshold voltages and operations are provided in the top table. Corresponding image with 5 × 5 μm size indicates bits 0 and 1. Therein, carrying of the full-adder requires further operation to V_C: V'_C = 3.5 V − V_C, where V_C = −1.5 or 3.5 V. Bottom panel shows the results of the electroluminescence of the single molecule, including that the right device serves as the sum and the left device serves as carry-out.

Figure 4. *Continued*
(E) Construction of the full-subtractor, in which *u* serves as minuend, *v* as subtrahend, and *w* as borrow in. Corresponding threshold voltages and operations are provided in the top table. Corresponding image with 5 × 5 μm size indicates bits 0 and 1. Bottom panel shows the results of the electroluminescence of the single molecule, including that the left device serves as the borrow out and the right device serve as the difference. Therein, borrowing of the full-subtractor requires further operation to V_C: $V'_C = 3.5\,V - V_C$, where $V_C = -1.5$ or 3.5 V.

heavy atom, i.e., by mixing between the single molecule and environment. Without isolation by using the CDs (Pt-MB was used), the added iodoethane[35] in PDMS increased spin-orbital coupling at the single-molecule site and the possibility of emitting phosphorescence photons (Figure 3F). For the integrated molecule in junctions, the relatively pure molecular state enables the desired photophysical characterizations, whereas mixing with the environment provides a more effective regulation strategy.

Binary logic operation via a single-molecule optoelectronic chip

Logic operations were further achieved based on efficient, tunable single-molecule electroluminescence. The alignment of the molecular orbital with the Fermi level of the electrodes can be regulated by the applied back gate voltage (V_G)[29] (Figures 2E and 4A), which affords tunable dark/bright states of the single-molecule device and enables further utilization for 0/1 logic operations. Among the electrical potentials of the source, drain, and gate electrodes, two could be chosen as the input terminals, and the other could be chosen as the regulatory terminal to switch the corresponding logic gate. In combination with the guidance of the V_{SD}-V_G two-dimensional mapping (Figure 4A; detailed description of the logic operation is provided in the supplemental information), all 16 basic logic gates were achieved in one single-molecule device (Figure S13), based on different input/regulatory terminals and the corresponding threshold voltages. Specifically, the bright states serving as bit "1" was marked by a green point by STORM (note that this does not represent the actual color of the emitted photons), whereas the dark states (serving as bit "0") could be observed. Taking the drain voltage (V_D) = 0 V as the regulatory terminal and defining the logic variables *u* and *v* by the threshold voltages of the source voltage (V_S) and V_G, respectively, False, *u*, NOT *u*, *v*, NOT *v*, AND, NOT AND (NAND), and inverse implication (NIMP) logic gates were demonstrated, guided by Figure 4A. Accordingly, by setting the V_D to other specific value, True, OR, NOT OR (NOR), and reverse inverse implication (RNIMP) logic gates can be obtained conveniently. Furthermore, exclusive OR (XOR), exclusive NOR (XNOR), implication (IMP), and reverse implication (RIMP) were demonstrated by taking $V_G = 0$ V as the regulatory terminal. All 16 basic logic gates agree with the Boolean function and can be further combined to afford a half-adder and half-subtractor (Figure S14). More specifically, the neighboring two single-molecule devices (Figures 4B and 4C) with voltage of terminal A (V_A) as the regulatory terminal, voltage of terminal B (V_B) as *u*, and V_G and voltage of terminal C (V_C) as *v* were designed (Figure S6), where the V_{SD} of the two devices were equal to $V_A - V_B$ and $V_C - V_B$, respectively. The half-adder and half-subtractor were demonstrated at the same two single-molecule devices by setting V_A as 0 and 2.5 V, respectively. Furthermore, in combination with an additional setting of the V_A and V_C terminals, the full-adder and full-subtractor were demonstrated (Figures 4D and 4E, respectively). Facilitated by the on-chip setup and device engineering, the multimodal electrical inputs enable comprehensive logic operations. Further preparation of a multifunctional logic circuit with high-integration density should consider constructing cascade circuits between the electrical and optical components.

Trinary logic operation via a single-molecule optoelectronic chip

The tunable multimodal photophysical process can be further applied for trinary logic variables beyond binary, which enables more effective operation. The dark, phosphorescence-emitting (which enables the location of the molecule by STORM

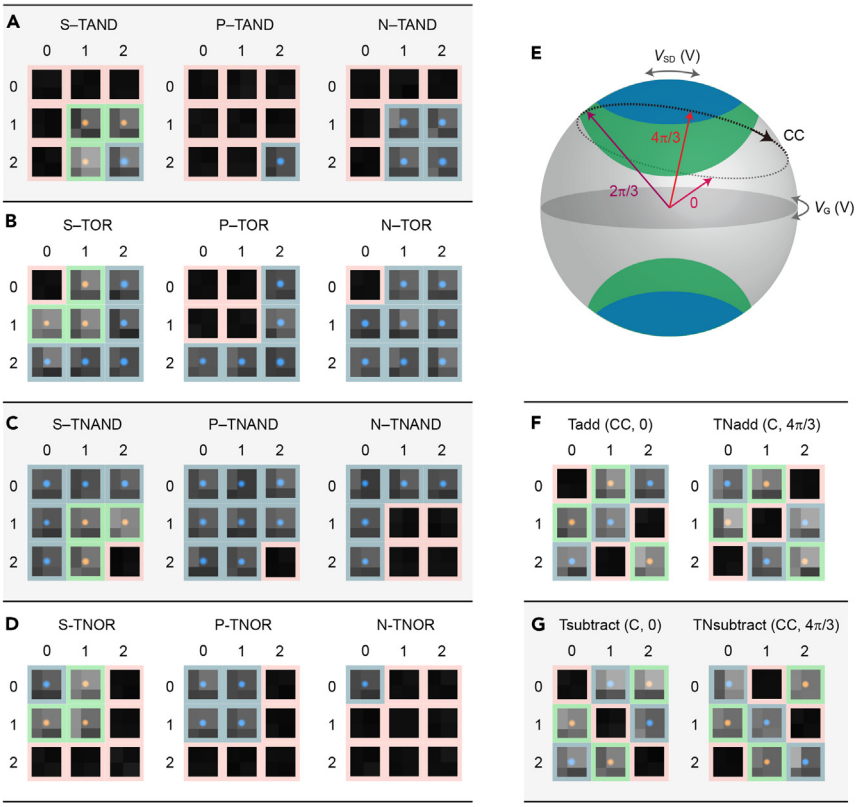

Figure 5. Trinary logic operations using a single-molecule Pt-MB@CD device

(A) Three types of TAND gates. Dark state, phosphorescence-emitting and mixed-emitting states were detected by a single-molecule spectroscopy, and the locations of the molecule are indicated by N/A and orange and blue points by STORM, respectively. Note that these colors do not represent the actual colors of the emitted photons. Corresponding super-high-resolution image with 100 × 100 nm size indicates bits 0–2, as in subsequent panels.

(B) Three types of trinary OR (TOR) gates.

(C) Three types of trinary NAND (TNAND) gates.

(D) Three types of trinary NOR (TNOR) gates.

(E) Spherical V_{SD} (range: −4 to 4 V) -V_G (range: 0 to 4 V) mapping as the reference for complex trinary operations.

(F) Tadd and TNadd operations based on the evolution of both V_{SD} and V_G, with different rotation directions and initial phase. C, clockwise. CC, counterclockwise.

(G) Tsubstract and TNsubstract operations based on the evolution of both V_{SD} and V_G, with different rotation directions and initial phase.

and is marked in orange; note that this does not represent the actual color of the emitted photons) and mixed-phosphorescence-fluorescence-emitting (which also enables the location of the molecule by STORM and is marked in blue) states can serve as bits "0," "1," and "2," respectively. Referring to the corresponding threshold voltages (Figure 4A), three types of trinary AND (TAND) operations were demonstrated (Figure 5A), indicating the multifunction of only one single-molecule device. The trinary logic operation enables 3^9 basic gates. Considering practicality, Figures 5B–5D and S15–S34 show the other typical gates, including detailed setups.[36] More importantly, the add or subtract operation can be achieved at only one device by trinary bits, which can be regarded as an alternative strategy to approach device minimalization. These logic operations are based on the evolution of both V_{SD} and V_G on the spherical V_{SD}-V_G mapping. Specifically, the logic variables can be set by the initial phase (0, 2π/3, and 4π/3) and rotation angle (0°, 120°, and 240°) on the evolution trajectory (Figure 5E). The change of the initial phase and

rotation direction afforded direct switching of the logic gates, including Tadd, TNadd, Tsubtract, and TNsubtract (Figures 5F and 5G). Figures S35–S38 show detailed setups. Therefore, facilitated by the balance between "pure" and "mixed" molecular states, trinary logic variables based on single-molecule tunable excited states were achieved, enabling logic operations with more information capability and corresponding reduction of device interconnections and the chip area.

Real-time communication via a single-molecule optoelectronic chip

Further precise tunability of only-phosphorescence or -fluorescence emission can be realized by the input of a programmable electrical sequence (Figure 6A). A lower bias voltage pulse can enable only-phosphorescence emission, whereas the timely removal of the triplet state by a gate voltage pulse can enable only fluorescence emission. More specifically, the singlet states prepared using a higher bias led to rapid fluorescent emission, whereas the long-lived triplet states can be quenched by the subsequent V_G pulse because of the electron transformation. Furthermore, to approach a relatively rapid phosphorescence response to the lower electrical pulse, the Pt-MB with 10^{-5} M externally added iodoethane was used (Figure 3F), concomitant with some loss of efficiency. Accordingly, energy-tunable photon emission can be applied for the precise transmission of information (Figures 6B–6E). The target information streams were designed by the programmable electrical pulse sequence with a 10-ms time interval and 1-ms pulse width (Figure 6E, enlarged at the right panel). The corresponding emitted photons were recorded synchronously (Figure 6D, enlarged at the right panel). The phosphorescence or fluorescence emission at set time intervals determines the binary information at the corresponding site, which can be adopted to transfer one-dimensional information by an American Standard Code for Information Interchange (ASCII) code table. As a single-photon source,[29] the single-molecule device can be further applied for encrypted message transmission (Figure S39 and Table S2). Furthermore, a combination of all the photon sequences enables the display of a two-dimensional graph, for example, the logo of the Peking University (Figure 6C). The tunable excited state facilitates the opportunities for future high-resolution display after integration.

The balance between pure and mixed molecular states is crucial for preparing tunable devices with inherent molecular properties. In this work, the isolation of the molecule from the environment by using two CDs enhanced the quantum yield of single-molecule electroluminescence and covalent coupling with electrodes enabled tunable excited states, which are essential to enabling all basic binary logic operations and typical trinary logic operations. In addition, facilitated by the single-molecule setup (avoiding intermolecular interactions), measurable electroluminescence and tunable lifetimes were also obtained without using the two CDs and were used for precise information transformation. This development of molecular and device engineering demonstrates the capability to link conceptual molecular electronics to practical semiconductors. In addition to logic operations and information communication, the multifunctional single-molecule optoelectronic chip provides a deep understanding of the single-molecule photophysical process and is an alternative optoelectronic strategy for constructing integrated nanocircuits beyond Moore's law.

EXPERIMENTAL PROCEDURES

Resource availability

Lead contact

Requests for further information and resources should be directed to and will be fulfilled by the lead contact, Xuefeng Guo (guoxf@pku.edu.cn)

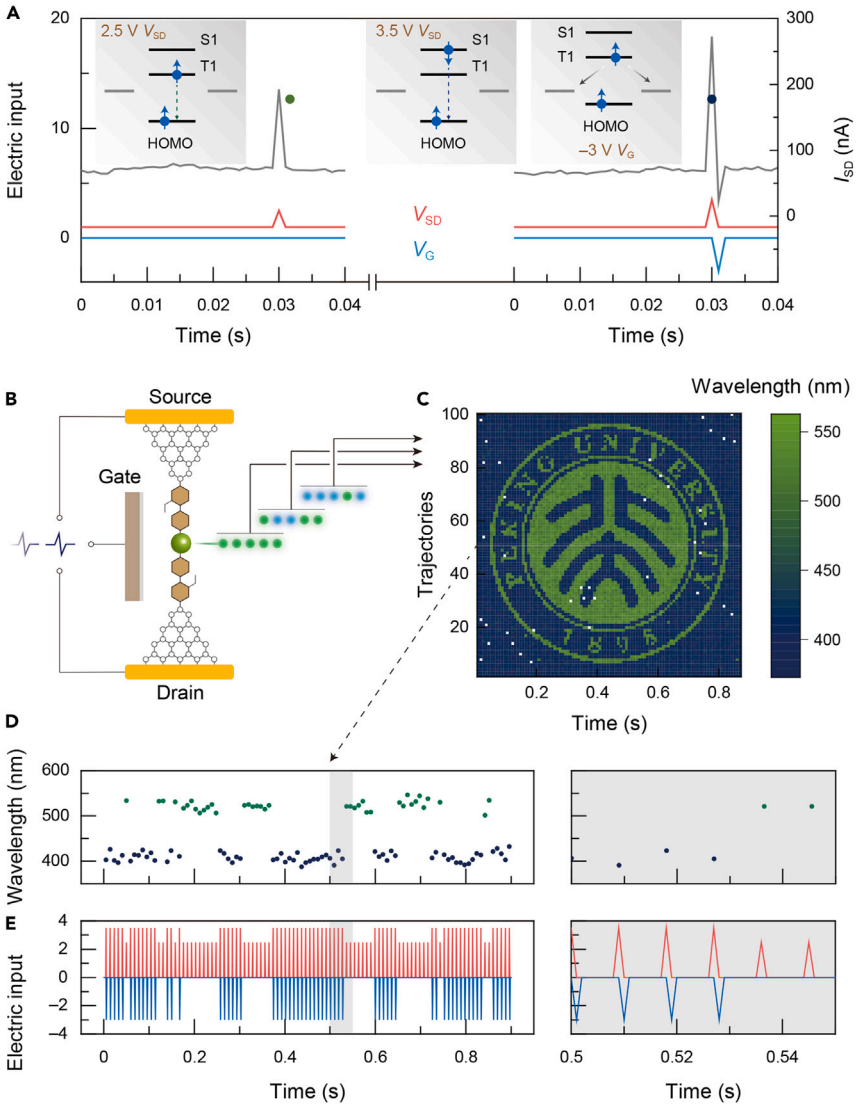

Figure 6. Real-time communication with a single-molecule Pt-MB device

(A) Selective emission of phosphorescence and fluorescence by designed V_{SD} or V_G electrical pulse sequences.

(B) Schematic of emitting information streams consisting of phosphorescence and fluorescence photons. The Pt-MB device with 10^{-5} M externally added iodoethane was used to enable a short lifetime (Figure 3F) for high-throughput information transmission.

(C) Output image (the logo of the Peking University) reconstructed from the emitted photons. When both fluorescence and phosphorescence were collected, the average wavelength of the fluorescence photons was used; when only phosphorescence was collected, the emission wavelength of the phosphorescence photons was used. The two-dimensional image was constituted by 100 one-dimensional photon sequences, where each one-dimensional photon sequence was obtained by the input of voltage sequences designed in advance. Permission for the use of the Peking University logo was obtained from the Peking University.

(D) One line of the output photons in (C) and the corresponding enlarged image.

(E) Measured input electrical pulse sequence with 10-ms resolution and the corresponding enlarged image.

Materials availability

The materials can be produced following the procedures in the section on synthesis and characterization in the supplemental information.

Data and code availability

Data from the GMG-SMJ measurements are available upon request from the lead contact.

SUPPLEMENTAL INFORMATION

Supplemental information can be found online at https://doi.org/10.1016/j.chempr.2024.01.005.

ACKNOWLEDGMENTS

We acknowledge primary financial supports from the National Key R&D Program of China (2021YFA1200101 and 2022YFE0128700), the National Natural Science Foundation of China (22150013 and 21933001), the New Cornerstone Science Foundation through the XPLORER PRIZE, the Natural Science Foundation of Beijing (2222009), and Frontiers Science Centre for New Organic Matter at Nankai University (63181206). C.Y. appreciates the support from the China National Postdoctoral Program for Innovative Talents (BX20220014), the National Natural Science Foundation of China (22303003), and the General Project of China Postdoctoral Science Foundation (2023M730049). Y.G. appreciates the support from the China National Postdoctoral Program for Innovative Talents (BX20230024) and the General Project of China Postdoctoral Science Foundation (2023M740065).

AUTHOR CONTRIBUTIONS

X.G. and J.T. conceived and designed the experiments. C.Y. and Y.G. fabricated the devices and performed the device measurements. H.M. synthesized the molecular bridges. J.J. and H.S. performed the transient luminescence experiments. X.G., C.Y., and Y.G. analyzed the data and wrote the manuscript. X.G., T.I., and J.T. discussed the results and commented on the manuscript.

DECLARATION OF INTERESTS

The authors declare no competing interests.

Received: August 13, 2023
Revised: November 12, 2023
Accepted: January 8, 2024
Published: January 25, 2024

REFERENCES

1. Edwards, C. (2021). Moore's Law: What comes next? Commun. ACM *64*, 12–14.
2. Su, T.A., Neupane, M., Steigerwald, M.L., Venkataraman, L., and Nuckolls, C. (2016). Chemical principles of single-molecule electronics. Nat. Rev. Mater. *1*, 16002.
3. Xin, N., Guan, J., Zhou, C., Chen, X., Gu, C., Li, Y., Ratner, M.A., Nitzan, A., Stoddart, J.F., and Guo, X. (2019). Concepts in the design and engineering of single-molecule electronic devices. Nat. Rev. Phys. *1*, 211–230.
4. Aviram, A., and Ratner, M.A. (1974). Molecular rectifiers. Chem. Phys. Lett. *29*, 277–283.
5. Xiang, D., Wang, X., Jia, C., Lee, T., and Guo, X. (2016). Molecular-scale electronics: From concept to function. Chem. Rev. *116*, 4318–4440.
6. Garner, M.H., Li, H., Chen, Y., Su, T.A., Shangguan, Z., Paley, D.W., Liu, T., Ng, F., Li, H., Xiao, S., et al. (2018). Comprehensive suppression of single-molecule conductance using destructive sigma-interference. Nature *558*, 415–419.
7. Jia, C.C., Migliore, A., Xin, N., Huang, S., Wang, J., Yang, Q., Wang, S., Chen, H., Wang, D., Feng, B., et al. (2016). Covalently bonded single-molecule junctions with stable and reversible photoswitched conductivity. Science *352*, 1443–1445.
8. Xin, N., Hu, C., Al Sabea, H., Zhang, M., Zhou, C., Meng, L., Jia, C., Gong, Y., Li, Y., Ke, G., et al. (2021). Tunable symmetry-breaking-induced dual functions in stable and photoswitched single-molecule junctions. J. Am. Chem. Soc. *143*, 20811–20817.
9. Sun, L., Diaz-Fernandez, Y.A., Gschneidtner, T.A., Westerlund, F., Lara-Avila, S., and Moth-Poulsen, K. (2014). Single-molecule electronics: from chemical design to functional devices. Chem. Soc. Rev. *43*, 7378–7411.
10. Song, H., Reed, M.A., and Lee, T. (2011). Single molecule electronic devices. Adv. Mater. *23*, 1583–1608.
11. Meng, L., Xin, N., Hu, C., Sabea, H.A., Zhang, M., Jiang, H., Ji, Y., Jia, C., Yan, Z., Zhang, Q., et al. (2022). Dual-gated single-molecule field-effect transistors beyond Moore's law. Nat. Commun. *13*, 1410.
12. Lörtscher, E. (2013). Wiring molecules into circuits. Nat. Nanotechnol. *8*, 381–384.
13. Richter, S., Mentovich, E., and Elnathan, R. (2018). Realization of molecular-based transistors. Adv. Mater. *30*, e1706941.

14. Song, H., Kim, Y., Jang, Y.H., Jeong, H., Reed, M.A., and Lee, T. (2009). Observation of molecular orbital gating. Nature *462*, 1039–1043.

15. Perrin, M.L., Burzurí, E., and van der Zant, H.S.J. (2015). Single-molecule transistors. Chem. Soc. Rev. *44*, 902–919.

16. Qiu, X.H., Nazin, G.V., and Ho, W. (2003). Vibrationally resolved fluorescence excited with submolecular precision. Science *299*, 542–546.

17. Xu, W., Li, R., Wang, C., Zhong, J., Liu, J., and Hong, W. (2022). Investigation of electronic excited states in single-molecule junctions. Nano Res. *15*, 5726–5745.

18. Marquardt, C.W., Grunder, S., Błaszczyk, A., Dehm, S., Hennrich, F., Löhneysen, H.V., Mayor, M., and Krupke, R. (2010). Electroluminescence from a single nanotube–molecule–nanotube junction. Nat. Nanotechnol. *5*, 863–867.

19. Zhang, K., Wang, C., Zhang, M., Bai, Z., Xie, F.F., Tan, Y.Z., Guo, Y., Hu, K.J., Cao, L., Zhang, S., et al. (2020). A Gd@C82 single-molecule electret. Nat. Nanotechnol. *15*, 1019–1024.

20. Li, J., Hou, S., Yao, Y.R., Zhang, C., Wu, Q., Wang, H.C., Zhang, H., Liu, X., Tang, C., Wei, M., et al. (2022). Room-temperature logic-in-memory operations in single-metallofullerene devices. Nat. Mater. *21*, 917–923.

21. Guo, Y., Yang, C., Zhou, S., Liu, Z., and Guo, X. (2022). A single-molecule memristor based on an electric-field-driven dynamical structure reconfiguration. Adv. Mater. *34*, e2204827.

22. Cao, Y., Dong, S., Liu, S., He, L., Gan, L., Yu, X., Steigerwald, M.L., Wu, X., Liu, Z., and Guo, X. (2012). Building high-throughput molecular junctions using indented graphene point contacts. Angew. Chem. Int. Ed. Engl. *51*, 12228–12232.

23. Rust, M.J., Bates, M., and Zhuang, X. (2006). Sub-diffraction-limit imaging by stochastic optical reconstruction microscopy (STORM). Nat. Methods *3*, 793–795.

24. Masai, H., Terao, J., Makuta, S., Tachibana, Y., Fujihara, T., and Tsuji, Y. (2014). Enhancement of phosphorescence and unimolecular behavior in the solid state by perfect insulation of platinum–acetylide polymers. J. Am. Chem. Soc. *136*, 14714–14717.

25. Russell, G.M., Inamori, D., Masai, H., Tamaki, T., and Terao, J. (2019). Luminescent and mechanical enhancement of phosphorescent hydrogel through cyclic insulation of platinum-acetylide crosslinker. Polym. Chem. *10*, 5280–5284.

26. Xiao, L., Chen, Z., Qu, B., Luo, J., Kong, S., Gong, Q., and Kido, J. (2011). Recent progresses on materials for electrophosphorescent organic light-emitting devices. Adv. Mater. *23*, 926–952.

27. Kubatkin, S., Danilov, A., Hjort, M., Cornil, J., Brédas, J.L., Stuhr-Hansen, N., Hedegård, P., and Bjørnholm, T. (2003). Single-electron transistor of a single organic molecule with access to several redox states. Nature *425*, 698–701.

28. Kuhnke, K., Große, C., Merino, P., and Kern, K. (2017). Atomic-scale imaging and spectroscopy of electroluminescence at molecular interfaces. Chem. Rev. *117*, 5174–5222.

29. Yang, C., Guo, Y., Zhou, S., Liu, Z., Liu, Z., Zhang, D., and Guo, X. (2023). A Tunable single-molecule light-emitting diode with single-photon precision. Adv. Mater. *35*, e2209750.

30. Kiguchi, M., Nakashima, S., Tada, T., Watanabe, S., Tsuda, S., Tsuji, Y., and Terao, J. (2012). Single-molecule conductance of π-conjugated rotaxane: new method for measuring stipulated electric conductance of π-conjugated molecular wire using STM break junction. Small *8*, 726–730.

31. Qian, H., Cousins, M.E., Horak, E.H., Wakefield, A., Liptak, M.D., and Aprahamian, I. (2017). Suppression of Kasha's rule as a mechanism for fluorescent molecular rotors and aggregation-induced emission. Nat. Chem. *9*, 83–87.

32. Baldo, M.A., and Forrest, S.R. (2000). Transient analysis of organic electrophosphorescence: I. Transient analysis of triplet energy transfer. Phys. Rev. B *62*, 10958–10966.

33. Bi, H., Palma, C.A., Gong, Y., Stallhofer, K., Nuber, M., Jing, C., Meggendorfer, F., Wen, S., Yam, C., Kienberger, R., et al. (2020). Electron–phonon coupling in current-driven single-molecule junctions. J. Am. Chem. Soc. *142*, 3384–3391.

34. Hellsing, B., Eiguren, A., Chulkov, E.V., and Echenique, P.M. (2005). Electron–phonon coupling and lifetimes of excited surface states. Surf. Sci. *593*, 12–18.

35. Graham-bryce, I.J., and Corkill, J.M. (1960). Use of solvents containing ethyl iodide in the investigation of phosphorescence spectra of organic compounds. Nature *186*, 965–966.

36. Gopal, P.V., Narkhede, S., and Sasikala, G. (2015). Implementation of Ternary Logic Gates using FGMOS. In 2015 International Conference on Smart Technologies and Management for Computing, Communication, Controls, Energy and Materials (ICSTM), pp. 275–279.